

Study on the Influence Law of Loading Rate on Soil Pressure Bearing Characteristics

Jian He, Dalin Wu, Jisheng Ma, Hongkai Wang and Yue Li

Abstract—The soil pressure bearing characteristics is used to calculate the sinkage, running resistance, vibration characteristic and traction characteristic when the vehicle travel on the soft road. The soil pressure-sinkage models take the Bekker's model as the representative used now are usually got with the low loading speed to the plate range from two centimeters per second to five centimeters per second and lack of research of soil pressure-sinkage characteristic under high loading speed. The paper studied the influence of high loading speed to the soil pressure-sinkage characteristic by plate sinkage test combined the numerical simulation and physical experiment. The numerical simulation considered the soil rate dependent constitutive model and inertial effect. The research results show that the higher loading speed can increase the soil pressure-sinkage characteristic and this influence reflect on the increase of soil deformation modulus. The pressure-sinkage model that considered the loading speed based with soil rate dependent coefficient λ on the Bekker's model was built. For the general soil, the value of soil rate dependent coefficient λ ranges from 0.07 to 0.18. The research conclusion can provide reference to the calculation of sinkage when the vehicle travels on the soft road.

Index Terms—Soil, Loading speed, Pressure-sinkage, Numerical simulation.

I. INTRODUCTION

THE research on the bearing characteristics of soil belongs to the research field of vehicle ground mechanics. Vehicle users (designers, dealers and researchers) need to know how to predict tractive performance of vehicles in a given soil condition of vehicle operations. Ability to predict tractive performance in a given soil condition of vehicle operations allows one to choose a proper vehicle and its design parameters, and also helps one to answer the main questions [1]:

- (1) How much drawbar pull can the vehicle produce in given soil, load and operating conditions?
- (2) What forward speed will be resulted for a given angular velocity of the drive wheels?
- (3) How much power does the vehicle need for moving?

A very important part of a track and wheel tractive

performance study is the sinkage and penetration force prediction which is necessary for obtaining vehicle traction, motion resistance, soil trafficability, soil compaction, rut depth, etc. The sinkage and penetration force prediction is to determine the relationship between normal stress p and vertical sinkage z of soil. The soil pressure bearing characteristics directly affect the subsidence and the driving resistance of the vehicle, which has important significance on the design of the vehicle structure and the prediction of the vehicle driving characteristics [2-4].

Since the development of vehicle ground mechanics, scholars from various countries have established some semi-empirical formulas through test methods to express the relationship between sinkage z and normal stress p , the typical ones are Bekker's soil index bearing model, the British Reece formula, and the former Soviet scholar Kuzkov's hyperbolic tangent model [5,6]. The widely used soil pressure model now was proposed by Bekker in the 1960s.

The soil bearing model proposed by the founder of vehicle ground mechanics Bekker [7,8] is:

$$p = \left(\frac{K_c}{b} + K_\phi \right) z^n \quad (1)$$

where K_c is the soil cohesion modulus, K_ϕ is the soil internal friction modulus, b is the short side length of plate and n represents the soil deformation coefficient.

The Bekker model is simple and the soil parameters are easily to be obtained, so it has been widely used since the 1960s. The coupling of the track shoes and the soft soil in the large-scale commercial dynamics simulation software ATV and Recurdyn is Bekker's soil pressure model. However, limited to experimental means, the plate loading speed conducted by Bekker with the range of $2\text{cm/s} \sim 5\text{cm/s}$, it lacks the research of higher loading speed [9].

Limited to experimental means, the plate loading speed conducted by researchers now is difficult to greater than 2cm/s , most tests are quasi-static.

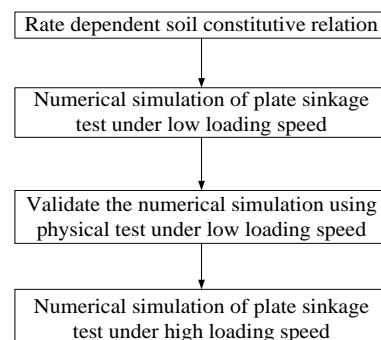


Fig.1 Research ideas of effect of high loading speed

Manuscript received April 12, 2019; revised July 16, 2019. This work was supported in part by the Key Research Subject of Army (Grant no. 404040602).

Corresponding author: Dalin Wu is with the Shijiazhuang Campus of Army Engineering University, Shijiazhuang, Hebei, P.C. 050000 China e-mail: dalinwu@163.com.

Jian He, Dalin Wu and Yue Li are with the Shijiazhuang Campus of Army Engineering University, Shijiazhuang, Hebei, P.C. 050000 China.

Jisheng Ma is with the Xijing Univeristy, Xian, Shanxi, P.C. 710123 China.

Hongkai Wang is with the Nanjing Campus of Army Academy of Artillery and Air Defense, Najing, Jiangsu, P.C. 211100 China.

The paper combined the numerical simulation with physical plate sinkage test to study the effect of higher loading speed to soil pressure sinkage characteristics. The research ideas of this subsection as shown in Figure.1

II. RATE DEPENDENT SOIL CONSTITUTIVE RELATION

A. Static constitutive model of soil

The constitutive relation of soil refers to the stress-strain relationship of soil. Soil is a typical elastoplastic material, and soil deformation is mainly based on plastic deformation. The plastic behavior of soil materials is different from the plastic behavior of metal materials in the stress dependence and dilatancy of soil materials [10].

A1. Elastic behavior

The generalized Hooke's law was used here to describe the elastic behavior of soil and two parameters namely the elastic modulus E and Poisson ratio ν are required for this. The generalized Hooke's law is given by

$$\sigma_{ij} = \frac{E}{1+\nu} \varepsilon_{ij} + \frac{\nu E}{(1+\nu)(1-2\nu)} \varepsilon_{kk} \delta_{ij} \quad (2)$$

where σ_{ij} is stress tensor, ε_{kk} is strain tensor and δ_{ij} is Kroneck-er delta, which can be written as

$$\delta_{ij} = \begin{cases} 1 \dots (i = j) \\ 0 \dots (i \neq j) \end{cases} \quad (3)$$

A2. Yield related with pressure

The process by which a material enters a plastic state from an elastic state is called a yielding process. The yield criterion is a criterion for judging whether a material enters a plastic state, and is an expression about a stress combination. For soil materials, yielding has significant pressure dependence, that is, when the confining pressure of the soil is increased, the yield limit is correspondingly increased, soil is a typical friction material. The ball stress and equivalent shear stress were used here to describe the yield of the soil material, as shown in Figure 2 [11].

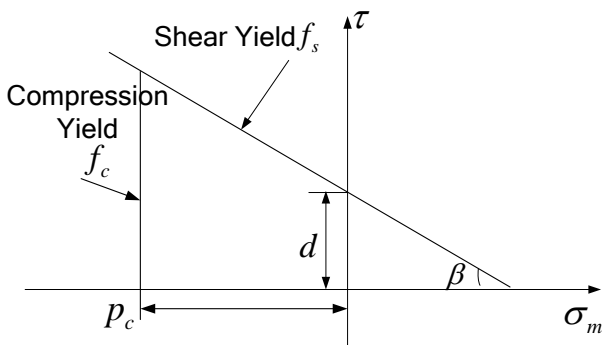


Fig.2 Yield surface of soil

The shear yield surface is given as:

$$f_s = \tau + \sigma_m \tan \beta - d = 0 \quad (4)$$

The compression yield surface is given as:

$$f_c = \sigma_m - p_c = 0 \quad (5)$$

where β and d are friction angle and cohesion of soil in the $\sigma_m - \tau$ plane, p_c is the isotropic compressive strength of soil. σ_m and τ are ball stress and equivalent shear stress as give by:

$$\begin{cases} \sigma_m = \frac{I_1}{3} = \frac{\sigma_{11} + \sigma_{22} + \sigma_{33}}{3} \\ \tau = \sqrt{J_2} = \sqrt{\frac{1}{2} s_{ij} s_{ij}} \end{cases} \quad (6)$$

where s_{ij} is deviatoric stress.

The β reflects the yield stress related with pressure of the soil and p_c can reflect the yield of soil due to isotropic compression, and this is very different from other metals.

A3. Flow rule

The flow rule is used to determine the direction of plastic strain increment of the soil when it enters the plastic deformation stage and that is the proportion of each component. Flow rules may be associated or non-associated. In the shear yield region, the plastic potential function is given as:

$$g_s = \tau + \sigma_m \tan \psi \quad (7)$$

where ψ represents dilatancy angle.

In the compression yield region, the plastic potential function is given as:

$$g_c = \sigma_m \quad (8)$$

Here for the shear yield surface, a non-associated flow was assumed and associated flow was used to the compression yield.

A4. Hardening law

The hardening law essentially is controlling the change in the size of yield surface. Here the equivalent plastic strain ε_{pl} was used to control the hardening behavior as shown in Figure 3 Each ε_{pl} corresponds to a yield surface.

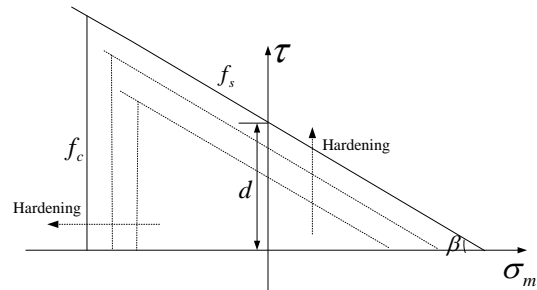


Fig.3 Hardening law

A5. Soil parameters

The parameters involved in this model are the elastic modulus E , Poisson ratio ν , friction angle β , dilatancy angle ψ , cohesion d and isotropic compressive strength p_c in the $\sigma_m - \tau$ plane. These parameters can all be obtained by the triaxial test of the soil. For triaxial stress conditions, the Mohr-Coulomb parameters, namely, the cohesion c and angle of friction φ can be converted to the angle of friction β and cohesion d in the $\sigma_m - \tau$ plane as follows [12]:

$$\begin{cases} \tan \beta = \frac{6 \sin \varphi}{\sqrt{3}(3 + \sin \varphi)} \\ d = \frac{6c \cos \varphi}{\sqrt{3}(3 + \sin \varphi)} \end{cases} \quad (9)$$

Here, the clay in Shijiazhuang was studied as shown in Figure 4 and used the triaxial test instrument as shown in Figure 5, Finally got the soil constitutive parameters as shown in Table I.



Fig.4 Clay in the Shijiazhuang area

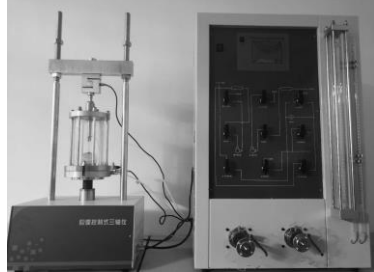


Fig.5 Triaxial test instrument

TABLE I

SOIL CONSTITUTIVE MODEL PARAMETERS

General		Plastic	
Density: 1923kg/m ³	Elastic	Friction angel: 47.3°	Dilation angel: 0°
Elastic modules: 5MPa	Poisson ratio: 0.32	Cohesion: 40150Pa	compressive strength: 210KPa

B. Rate dependent effect of soil

Rate dependent effect of soil means the law that yield stress increased with the loading speed increased [13-15].

Assumed the soil stress-strain relation at quasi-static state can be written as:

$$\sigma_{ij} = f^0(\varepsilon_{ij}) \quad (10)$$

where σ_{ij} and ε_{ij} are stress tensor and strain tensor, f^0 is the relation function.

So the soil stress-strain relation considered the strain rate can be written as:

$$\sigma_{ij} = f^0(\varepsilon_{ij})R(\dot{\varepsilon}_{ij}) \quad (11)$$

where $\dot{\varepsilon}_{ij}$ is the strain rate, $R(\dot{\varepsilon}_{ij})$ is the ratio between dynamic state to the quasi-static state. The numerical value of reflects the soil strain rate effect. Two methods were used in numerical simulation to define $R(\dot{\varepsilon}_{ij})$, one was to directly input the value of ratio corresponding to strain rate in the form of a table, the other one was define an expression between them, typical were power and exponential functions.

The power function form was represented by Cowper-Symonds equation:

$$\dot{\varepsilon}_{ij} = D(R-1)^n \quad (12)$$

The exponential function form was represented by Johnson-Cook equation:

$$\dot{\varepsilon}_{ij} = \varepsilon_0 e^{\left[\frac{1}{C}(R-1)\right]} \quad (13)$$

The D, n, ε_0 and C are material parameters.

The soil strain rate parameter here was got by shear test used direct shear test instrument as shown in Figure 6. The shear speed of instrument range from 0.001-2.4mm/min ,

the different shear speed were conducted.



Fig.6 Direct shear testing equipment

Finally got the soil strain rate dependent effect parameter is shown in Table II.

TABLE II
SOIL RATE DEPENDENT EFFECT PARAMETER

Yield Stress ratio	Equivalent strain rate
1	0.002
1.1	0.02
1.21	0.2

C. Soil inertia effect

Inertia effect refers to the material properties related to quality. The general vibration differential equation is shown in Equation (14).

$$m \ddot{x} + c \dot{x} + kx = F \quad (14)$$

where m is mass matrix, c is damping matrix, k is stiffness matrix, x, \dot{x} and \ddot{x} are displacement matrix, velocity matrix and acceleration matrix, F is external load matrix.

D. Program the soil constitutive relation

The VUMAT subroutine was used here to combine the soil constitutive relation with the finite element analysis software ABAQUS, the program flow is as shown in Figure 7.

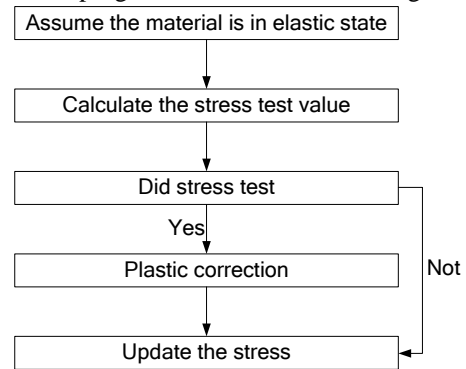


Fig.7 Program flow of soil constitutive relation

D1. Stress test value

First, assume the material in the elastic state, calculate the stress test value at t^{n+1} time:

$$^* \sigma_{ij}^{n+1} = \sigma_{ij}^n + \bar{\sigma}_{ij}^- \Delta t \quad (15)$$

where σ_{ij}^n is the stress tensor at t^n time, $^* \sigma_{ij}^{n+1}$ is the stress test value tensor at t^{n+1} time, $\bar{\sigma}_{ij}^-$ is the stress rate and Δt is time increment.

The Jaumann stress rate was used here for the reason that Cauchy stress rate is relevant with the rigid body rotation and not is an objective tensor, the final stress test value can be written as:

$${}^* \sigma_{ij}^{n+1} = \sigma_{ij}^n + 2G \Delta \varepsilon_{ij} + \left(K - \frac{2}{3}G\right) \Delta \varepsilon_m \delta_{ij} \quad (16)$$

where K and G are volume deformation modulus and shear modulus, $\Delta \varepsilon_{ij}$ is strain increment tensor and $\Delta \varepsilon_m$ is ball strain increment.

Further combined the Equation (6) then the ball stress test value ${}^* \sigma_m^{n+1}$ and equivalent shear stress test value ${}^* \tau^{n+1}$ can be written as:

$${}^* \sigma_m^{n+1} = \frac{{}^* \sigma_{11} + {}^* \sigma_{22} + {}^* \sigma_{33}}{3} \quad (17)$$

$${}^* \tau^{n+1} = \sqrt{\frac{1}{2} {}^* s_{ij}^{n+1} {}^* s_{ij}^{n+1}}$$

D2. Stress test

Combined Equation (17) with Equation (4) (5), and did the stress test according to the Figure 2:

(1) When $f_s({}^* \sigma_m^{n+1}, {}^* \tau^{n+1}) > 0$, the stress point beyond the yield surface and expressed as shear yield, then did the plastic correction and used g_s to determine the flow rule.

(2) When $f_s({}^* \sigma_m^{n+1}, {}^* \tau^{n+1}) < 0$ and $f_c({}^* \sigma_m^{n+1}, {}^* \tau^{n+1}) < 0$, the stress point beyond the yield surface and expressed as compression yield, then did the plastic correction and used g_c to determine the flow rule.

(3) When $f_s({}^* \sigma_m^{n+1}, {}^* \tau^{n+1}) < 0$ and $f_c({}^* \sigma_m^{n+1}, {}^* \tau^{n+1}) > 0$, the stress point into yield surface that means the elastic state and do not need the plastic correction.

D3. Plastic correction

(1) Shear yield plastic correction

g_s was used here to determine the flow rule and the corrected stress should return to the $f_s({}^* \sigma_m^{n+1}, {}^* \tau^{n+1}) = 0$, the plastic scale factor can be written as Equation (18) through the calculation.

$$d\lambda_s = \frac{f_s({}^* \sigma_{ij}^{n+1})}{G + K \tan \beta \tan \psi} \quad (18)$$

Then the corrected ball stress can be written as:

$$\sigma_m^{n+1} = {}^* \sigma_m^{n+1} - K \tan \psi d\lambda_s \quad (19)$$

For the reason that $f_s({}^* \sigma_m^{n+1}, {}^* \tau^{n+1}) = 0$, so the corrected equivalent shear stress can be written as:

$$\tau^{n+1} = d - \sigma_m^{n+1} \tan \beta \quad (20)$$

(2) Compression yield plastic correction

g_c was used here to determine the flow rule and the corrected stress should return to the $f_c({}^* \sigma_m^{n+1}, {}^* \tau^{n+1}) = 0$, the plastic scale factor can be written as Equation (21) through the calculation.

$$d\lambda_c = \frac{f_c({}^* \sigma_{ij}^{n+1})}{K} \quad (21)$$

Then the corrected ball stress can be written as:

$$\sigma_m^{n+1} = p_c \quad (22)$$

The corrected ball stress was satisfied with the $f_c({}^* \sigma_m^{n+1}, {}^* \tau^{n+1}) = 0$ so the equivalent shear stress did not been corrected and corrected equivalent shear stress can be written as:

$$\tau^{n+1} = {}^* \tau^{n+1} \quad (23)$$

D4. Update stress

Accorded to the stress return algorithm, scale the equivalent shear stress test value ${}^* \tau^{n+1}$, then the final stress tensor at t^{n+1} time was:

$$\sigma_{ij}^{n+1} = {}^* s_{ij}^{n+1} \frac{\tau^{n+1}}{{}^* \tau^{n+1}} + \sigma_m^{n+1} \delta_{ij} \quad (24)$$

III. LOW LOADING SPEED SIMULATION

A. Finite element model

Here, the clay in Shijiazhuang area was taken as the research object, and a plate was pressed into the soil to study the whole sinkage process through numerical simulation.

The choice of the size of the soil area affects the calculation time and calculation accuracy. If the soil area is too small, the calculation result will be incorrect. If the soil area is too large, the calculation time will be increased. Considered the boundary effect of the whole plate pressed process, took the soil analysis area as a cube with a side length of 1m. In order to save computer computing time, the model was modeled for the symmetry of the length and width directions according to the symmetry. Subdivisions the mesh in the area close to the plate further to improve the calculation efficiency [16]. The final model is shown in Figure 8. The entire finite element model was divided into 1204,000 finite elements. An 8-node linear brick element with reduced integration and hourglass control and a structured mesh was used [17].

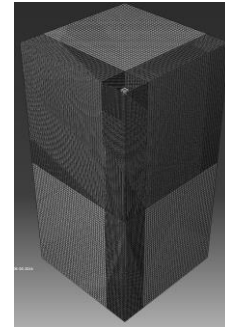


Fig.8 Finite element model of plate sinkage test

B. Sinkage test simulation

The loading speed was 0.2 cm/s , the stress distribution at the loading process as shown in Figure 9.

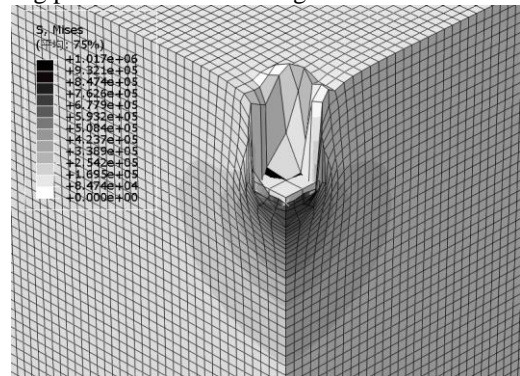


Fig.9 Mises stress nephogram of plate sinkage test

From the stress distribution of the soil region in Figure 9, the stress distribution showed a shape of pressure bubbles with outward expansion, this is consistent with the Boussinesq solution.

The relations between plate sinkage and pressure obtained from the simulation are as shown in Figure 10.

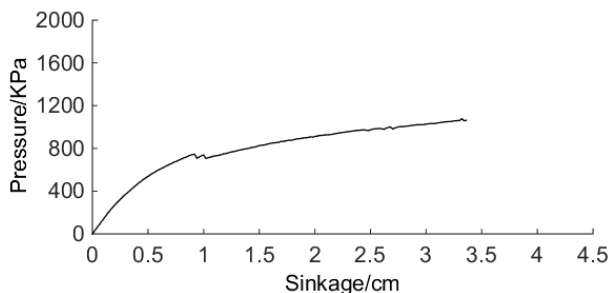


Fig.10 Pressure-sinkage curve of numerical simulation results

The sinkage curve has three distinct stages, namely (1) linear deformation stage: the relationship between load and sinkage is linear in this stage and the major part of the sinkage is caused by soil compaction. (2) local shear failure stage: in this stage, with the increase in load, the relationship between load and sinkage is represented by a downward curve, and in this stage, in addition to the soil compaction plastic deformation also occur in some parts of the soil as the shear stress exceeds the shear strength in these areas. (3): complete failure stage: when the load continues to increase to a critical value, soil sinkage also increases rapidly as the soil under the plate has already failed and cannot continue to bear more load. This critical value is called ultimate bearing capacity.

IV. VALIDATE THE SIMULATION RESULTS

A. Plate sinkage instrument

The results of numerical simulations require physical testing to verify. The plate sinkage test conducted before mainly have two types:

- (1) Soil bin test in laboratory as shown in Figure11.

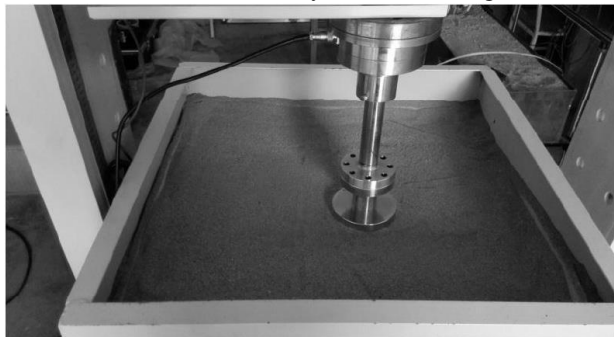


Fig.11 Soil bin test device

- (2) Bekker sinkage test in filed, the working principle as shown in Figure 12.

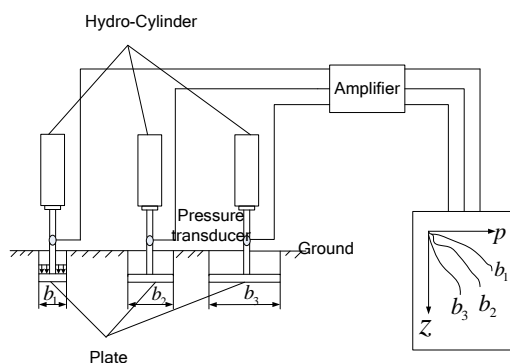


Fig.12 Working principle of Bekker sinkage device

The comparison of two instruments is as shown in table III. the soil bin test can cause the disturbance to the field soil and the soil properties will change. The Bekker sinkage instrument do test in the field so it is efficient and accurate but

it needs huge instrument and not easy to use.

TABLE III
COMPARISON OF PLATE SINKAGE DEVICES

	Advantages	Disadvantages
Soil bin test instrument	Controllable test conditions	Soil disturbance
Bekker sinkage instrument	Efficient	Huge instrument

For above reasons, a simple and convenient plate sinkage device was designed here as shown in Figure 13.



Fig.13 Plate sinkage device

The simple and convenient plate sinkage device did the test in field, used screw system to apply load, pressure transducer to measure the load, caliper to measure the sinkage, penetrated eight drilling steel to soil to resistant the reacting force of plate.

B. Physical test

Did the physical plate sinkage test use the device (at Figure13) as shown in Figure 14 , recorded data every five millimeters when the plate sinkage. The test results are shown in Table IV.



Fig.14 Plate sinkage physical test

TABLE IV
PHYSICAL TEST RESULTS

Sinkage (mm)	Pressure (kg)	Sinkage (mm)	Pressure (kg)
5	55	25	148
10	90	30	155
15	120	35	161
20	136	40	163

C. Comparison between numerical simulation and physical test results

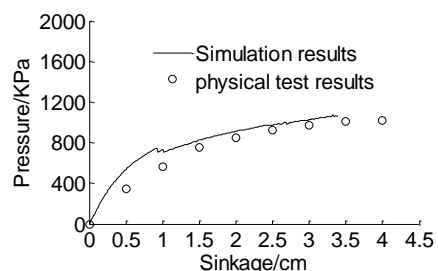


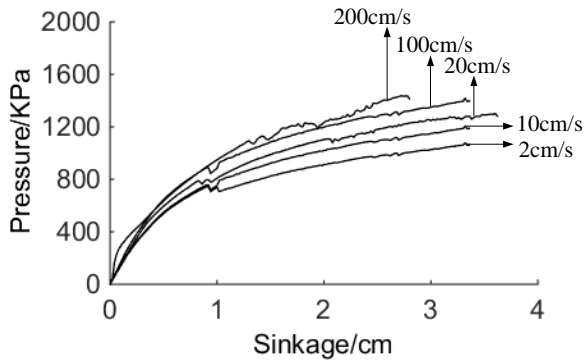
Fig. 15 Verification of numerical simulation results

Put the simulation results and physical results in Figure 15. From the Figure 15, one can see that simulation results were

consistent with the data got by physical test, this validated the effectiveness of the finite element model built. Then the high loading speed to plate was analyzed based on the verified finite element model.

V. HIGH LOADING SPEED SIMULATION

Separately set the loading speed as 2 cm/s , 10 cm/s , 20 cm/s , 100 cm/s and 200 cm/s , through simulation got the sinkage-pressure curves as shown in Figure 16.



16 Pressure-sinkage curves under different loading speed

It can be seen from Figure 13 that as the loading speed increases, the pressure value corresponding to the same soil sinkage increases, that is, the increase of the loading speed increases the pressure bearing capacity of the soil. To further analyze the law, the pressure and sinkage relations are plotted in logarithmic coordinates, as shown in Figure 17.

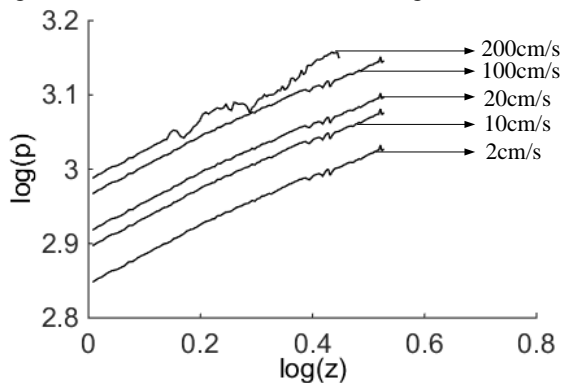


Fig.17 Pressure-sinkage curves under different loading speed at logarithmic coordinates

Conversion the coordinates to logarithmic, the equation to describe the relation between soil sinkage and vertical load as Equation (1) can be written as

$$\lg p = \lg \left(\frac{K_c}{b} + K_\phi \right) + n \lg z \quad (25)$$

Equation (25) shows the slope of curves at logarithmic coordinates represents the soil deformation coefficient n , the intercept of curves represents the soil deformation modulus.

The curves in Figure 17 have almost the same slope that shows the soil deformation coefficient unchanged under different loading speed. The intercept increase with the higher loading speed shows that the soil deformation modulus increase.

To further study the effect of loading speed to soil deformation modulus, draw the relation between soil deformation modulus and loading speed in logarithmic coordinates as shown in Figure 18.

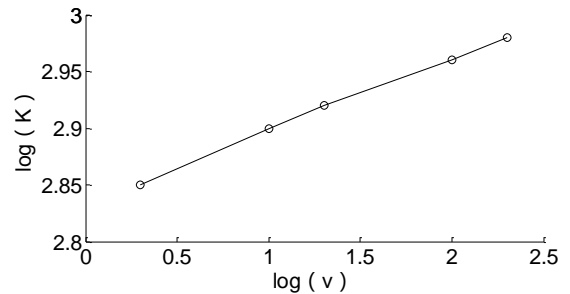


Fig.18 Relation curve between soil deformation modulus and loading speed

Form the Figure 18, one can see that a linear relationship exists between soil deformation modulus and loading speed in logarithmic coordinates.

VI. PRESSURE-SINKAGE MODEL CONDIRE LOADING SPEED

A. Model

From Figure 14, it can be concluded that:

$$\lg K - \lg K_{ref} = \lambda (\lg v - \lg v_{ref}) \quad (26)$$

where λ is the slope of the curve in figure 19 namely soil rate dependent parameter, K is the soil deformation modulus under the loading speed v , K_{ref} is the reference soil deformation modulus under reference loading speed v_{ref} .

Equation (11) can also be written as:

$$K = K_{ref} \times \left(\frac{v}{v_{ref}} \right)^\lambda \quad (27)$$

Combined the Equation (1), then the soil pressure-sinkage model considered loading speed can be written as:

$$p = \left\{ \left(\frac{K_c}{b} + K_\phi \right)_{ref} \times \left(\frac{v}{v_{ref}} \right)^\lambda \right\} z^n \quad (28)$$

where $\left(\frac{K_c}{b} + K_\phi \right)_{ref}$ is the reference soil deformation modulus under reference loading speed v_{ref} , $\left(\frac{v}{v_{ref}} \right)^\lambda$ is the term considered the loading speed, λ is the rate dependent coefficient.

When the value of rate dependent coefficient λ is zero, then the Equation (13) will degenerate into Equation(1). The pressure-sinkage model considered loading speed degenerate into Bekker model.

B. Model parameter value λ ranges

The soil rate dependent coefficient λ should positively correlated with the soil strain rate parameter $R(\dot{\epsilon}_{ij})$, the results of some existing soil strain rate parameters are shown in Table V.

TABLE V
RESULTS OF SOME EXISTING SOIL STRAIN RATE PARAMETERS

Soil sample	Soil strain rate parameter	Test method	References
Artificial clay	1.1	Cross plate cut	Bisoton [18]
Lyndhurst	1.194	Triaxial	Graham [19]
Burswood	1.275	Penetration	Chuang [20]
Onsoy	1.38	Penetration	Yafate [21]

The results show that the value of soil strain rate parameter $R(\dot{\varepsilon}_{ij})$ ranges from 1.1 to 1.38.

When the soil strain rate parameter $R(\dot{\varepsilon}_{ij})$ is the lower limit 1.1, the soil rate dependent coefficient λ is 0.07 where can be got from Figure 18.

When the soil strain rate parameter $R(\dot{\varepsilon}_{ij})$ is the upper limit 1.38, through the simulation and got the soil rate dependent coefficient λ is 0.18.

In summary, for the general soil, the value of soil rate dependent coefficient λ ranges from 0.07 to 0.18.

VII. CONCLUSION

- 1) The soil has a significant rate effect, and the increase of the loading rate will enhance the pressure bearing characteristics of the soil.
- 2) High loading speed can enhance the soil pressure bearing characteristics by increase the soil deformation modulus , it can be described by the term $(\frac{v}{v_{ref}})^2$. The soil pressure bearing model considered the loading speed based on the Bekker's theory is shown in equation (28).
- 3) For the soft clay in Shijiazhuang area studied in this paper, when the loading rate increases by an order of magnitude corresponding to a 10% increase in soil yield strength, the rate dependent coefficient λ is 0.07. For the general soil, the value of soil rate dependent coefficient λ ranges from 0.07 to 0.18.

REFERENCES

- [1] Modest Lyasko, "LSA Model for Sinkage Predictions", *Journal of Terramechanics*, vol. 47, pp. 1-19, 2010.
- [2] K. J. Zhang, "Vehicle Terramechanics". *Beijing: National Defense Industry Press*, pp. 143-150, 2002.
- [3] C. B. Yang, "Research on the adhesion property of high-speed track on soft ground and optimization of track shoe". *Beijing: Beijing Institute of Technology*, pp. 1-10, 2015.
- [4] X. G. Zhu, "Coupling dynamic characteristic research for wheels-track-terrain system of high-speed tracked vehicles". *Beijing: Beijing Institute of Technology*, pp. 15-20, 2015.
- [5] A. R. Reece, "Problems of Soil-Vehicle Mechanics". *US Army L L L, ATAC, No 8479, Warren, Mich*, pp. 23-50, 1964.
- [6] S. M. Yang, "Ground Mechanics and Working Theory of Engineering Machinery". *Beijing: China Communications Press*, pp. 55-64, 2010.
- [7] M. G. Bekker, "Off-Road Locomotion". *Ann Arbor, Michigan: The University of Michigan Press*, pp. 78-90, 1960.
- [8] M. G. Bekker, "Introduction to Terrain-Vehicle Systems". *Ann Arbor, Michigan: The University of Michigan Press*, pp. 101-120, 1969.
- [9] J. He, J. S. Ma and D. L. Wu. "A review of development and current study of vehicle terramechanics". *Journal of Gun Launch & Control*, vol.38, pp 89-93, 2017.
- [10] X. P. Chen, "Constitutive Relation of Soils". *Beijing: China Water and Power Press*, pp 15-60, 2010.
- [11] P. Huang, "Material point method for metal and soil impact dynamics problems". *Beijing: Tsinghua University*, pp.113-135, 2010.
- [12] Y. R. Zheng, "Generalized Plastic Mechanics-Principle of Plastic Mechanics of Rock and Soil". *Beijing: China Architecture & Building Press*, pp. 11-15, 2002.
- [13] J. Liu, M.Z. Li and C. C. Han, "Influence of soil strain-rate effect on embedment depth of dynamically installed anchors". *Journal of Dalian University of Technology*, vol.57, pp 68-77, 2017.
- [14] K. Fei, "Applied Abaqus in Geotechnical Engineering". *Beijing: China Water and Power Press*, pp. 20-35, 2013.

- [15] H. Sam, "Applied Soil Mechanics with Abaqus Applications". *Canada: John Wiley and Sons, Inc*, pp. 57-65, 2013.
- [16] Elzbieta Gawronska, Robert Dya and Norbert Sczygiol, "Numerical Simulations of Stress Distribution in Complex Structures with Various Average Volume Fraction". *Proceedings of The World Congress on Engineering and Computer Science*, pp. 667-681, 2018.
- [17] Pantira Klankaew and Nopparat Pochai, "Numerical Simulation of Nonlinear Thin Fluid Film Flow Velocity Model of a Third Grade Fluid on a Moving Belt using Finite Difference Method with Newton Iterative Scheme". *Proceedings of The International MultiConference of Engineers and Computer Scientists*, pp. 318-321, 2019.
- [18] G. Biscontin, J. M. Pestana, "Influence of Peripheral Velocity on Vane Shear Strength of An Artificial Clay". *Geotechnical Testing Journal*, vol. 24, pp. 423-429, 2001.
- [19] J. Graham, J.H. Crooks and A.L. Bell, "Time Effects on the Stress-Strain Behaviour of Natural Soft Clays". *Geotechnique*, vol. 33, pp. 327-340, 1983.
- [20] S.F. Chung, M.F. Randolph and J.A. Schneider, "Effect of Penetration Rate on Penetrometer Resistance in Clay". *Journal of Geotechnical and Geoenvironmental Engineering*, vol. 132, pp. 1188-1196, 2006.
- [21] N.J. Yafate and J.T. Dejong, "Influence of Penetration Rate on Measured Resistance with Full Flow Penetrometers in Soft Clay". *Geotechnical Special Publication*, vol. 173, pp. 1-10, 2007.